Nonlinear Analysis and Control of Interleaved Boost Converter using Real Time Cycle to Cycle Variable Slope Compensation

Haimeng Wu*, *Member, IEEE*, Volker Pickert*, *Member, IEEE*, Damian Giaouris*, *Member, IEEE*
Bing Ji+ *Member, IEEE*
*School of Electrical and Electronic Engineering, Newcastle University
+ Department of Engineering, University of Leicester

***Abstract*— Switched-mode power converters are inherently nonlinear and piecewise smooth systems which may exhibit a series of undesirable operations that can greatly reduce the converter's efficiency and lifetime. This paper presents a nonlinear analysis technique to investigate the influence of system parameters on the stability of interleaved boost converters. In this approach, Monodromy matrix which contains all the comprehensive information of converter parameters and control loop can be employed to fully reveal and understand the inherent nonlinear dynamics of interleaved boost converters, including the interaction effect of switching operation. Thereby not only the boundary conditions but also the relationship between stability margin and the parameters given can be intuitively studied by the eigenvalues of this matrix. Furthermore, employing the knowledge gained from this analysis a real-time cycle to cycle variable slope compensation method is proposed to guarantee a satisfactory performance of the converter with an extended range of stable operation. Outcomes show that systems can regain stability by applying the proposed method within a few time periods of switching cycles. The numerical and analytical results validate the theoretical analysis, and experimental results verify the effectiveness of the proposed approach.**

***Index Terms*— Nonlinear analysis, bifurcation control, interleaved boost converter, Monodromy matrix, variable slope compensation**

I. Introduction

Due to the benefits of current ripple cancellation, passive components size reduction, and improved dynamic response contributed by interleaving techniques [1-3], interleaved switch-mode power converters are widely used in power systems such as electric vehicles [4], photovoltaics power generation [5] and thermoelectric generator systems [6]. However, in spite of the widespread applications of this type of DC-DC converter, their nonlinear effects due to sequential switching operations have not been sufficiently considered in converter design.

Manuscript received June 08, 2016; revised September 12, 2016; accepted October 24, 2016. Date of current version October 31, 2016. This work is sponsored by Vehicle Electrical Systems Integration (VESI) project (EP/I038543/1), which is funded by the Engineering and Physical Sciences Research Council (EPSRC). It is also supported in part by the scholarship from China Scholarship Council (CSC).

H. Wu, V. Pickert, and D. Giaouris are with the School of Electrical and Electronic Engineering, Newcastle University, Newcastle upon Tyne, United Kingdom, (e-mail: Haimeng.wu@ncl.ac.uk, Volker.pickert@ncl.ac.uk, Damian.Giaouris@ncl.ac.uk).

B.Ji is with the Department of Engineering, University of Leicester, Leicester, United Kingdom (email: Bing.ji@le.ac.uk)

In general, DC-DC converters are piecewise smooth systems and their dynamic operations show a manifestation of various nonlinear phenomena, as evidenced by sudden changes in operating region, bifurcation and chaotic operation when some circuit parameters are varied [7, 8]. For example, it is possible to have a sudden increase in the current ripple and then it forces the converter to operate in forbidding current/voltage areas with adding low frequency, high amplitude components. These unexpected random-like behaviors potentially lead to a violation of designated operation contours, increased electromagnetic interference (EMI), reduced efficiency and in the worst-case scenario a loss of control with consequent catastrophic failures. Unfortunately, all these phenomena cannot be predicted (and hence avoided) by using conventional linearized model of the converter. Without the thorough knowledge of the existing circuits, experience-based trial and error procedure is often applied in practice to restrain operating point within the safe operating region. As a result, circuit design criteria are always determined by selective ballpark values of components and parameters based on lessons learned from the past rather than applying an appropriate systematic design methodology.

A. Stability Analysis Methods for Power Converters

To study and analyze the inherent stability of power converters, most power electronics practitioners conventionally employ the linearized averaging technique to fit the analysis of power converter into the framework of linear systems theory, and thus discontinuities introduced by the switching action of the circuit are ignored [9, 10]. This gives a simple and accurate model for steady-state and dynamic response at timescale much slower than switching cycles but fails to encompass nonlinear behavior at a fast timescale as the switching action itself makes the converter model to be a highly nonlinear system.

Researchers had shown endeavor to develop the conventional averaging methodology and thus it was extended to frequency-dependent averaged models by taking into account of the effect of fast-scale dynamics [11]. A multi-frequency averaging approach was then proposed to improve the conventional state-space averaging models [12], modeling the dynamic behavior of DC–DC converters by applying and expanding the frequency-selective averaging method [13]. An analysis method based on the Krylov-Bogoliubov-Mitropolsky (KBM) algorithm was developed to recover the ripple components of state variables from the averaged model [14]. However, such improved models have some limitations to describe chaotic dynamics completely and effectively. To address fast-scale nonlinearities, discrete nonlinear modeling is the most widely used approach. Nonlinear map-based modeling [15] developed from sampled-data modeling [16] in the early stages applies an iterative map for the analysis of system stability which is obtained by sampling the state variables of the converter synchronously with PWM clock signals. This method is commonly referred to as the Poincaré map method. Stability is indicated by the eigenvalues of the fixed point of the Jacobian of the map, even though in some cases the map itself cannot be derived in closed-form because of the transcendental form of the system's equations. Hence the map has to be obtained numerically.

Other alternative approaches such as Floquet theory [17], Lyapunov-based methods [18] and trajectory sensitivity approach [19] are applied effectively for the nonlinear analysis of power converters. Specifically, the evolution of perturbation is studied directly in Floquet theory to predict the system's stability, by deriving the absolute value of the eigenvalues of the complete cycle solution matrices. In Lyapunov-based methods, piecewise linear Lyapunov functions are searched and constructed to describe the system's stability. For trajectory sensitivity approach, systems are linearized around a nominal trajectory rather than around an equilibrium point and the stability of the system can be determined by observing the change in a trajectory due to small initial or parameters variation. There have been combined approaches developed from combining state-space averaging and discrete modeling. Examples of these methods are design-oriented ripple-based approach [20, 21]; Takagi–Sugeno (TS) fuzzy model-based approach [22] and system-poles approach [23]. Apart from aforementioned approaches, other individual methods, such as symbolic approach [24] and energy balance model [25] were proposed to analyze the nonlinearities of switching power converters. A recent review paper on stability analysis methods for switching mode power converters has summarized some approaches presented [26].

B. Control of Nonlinearity in Power Converters

Various control techniques are proposed to tackle nonlinear behaviors based on the above methodologies, which can be classified into two categories: feedback-based and non-feedback based techniques. In the feedback-based group, a small time-dependent perturbation is tailored to make the system operation change from unstable periodic orbits (UPOs) to targeted periodic orbits. Ott-Grebogi-Yorke (OGY) approach proposed by Ott et al [27] was the first well-known chaos control method. One advantage of this method is that a priori analytical knowledge of the system dynamics is not required, which makes it easier to implement [28]. Then Delayed Feedback Control (TDFC) methods were proposed to stabilize the UPOs in the field of nonlinear dynamics [29, 30]. In this method, the information of the current state and prior one-period state is used to generate signals for the stabilizing control algorithm. Washout filter-aided feedback control was proposed to address the Hopf bifurcation of dynamic systems [31]. Other filter-based non-invasive methods for the control of chaos in power converters have also been proposed [32]. Apart from the aforementioned control methods, a self-stable chaos-control method [33], predictive control [34] and frequency-domain approach [35] have been proposed to eliminate bifurcation and chaotic behavior in various switching DC-DC converters.

In the non-feedback category, the control target is not set at the particular desired operating state, whereas the chaotic system can be converted to any periodic orbit. Resonant parametric perturbation is one of the most popular methods [36, 37]. In this approach, some parameters at appropriate frequencies and amplitude are normally perturbed to induce the system to stay in stable periodic regions, converting the system dynamic to a periodic orbit. Other examples of this type of method include the ramp compensation approach [38], fuzzy logic control [39] and weak periodic perturbation [40]. Compared to feedback-based methods, no online monitoring and processing are required in a non-feedback approach, which makes it easy to implement and suitable for specific practical applications.

However, in spite of the various approaches available, the most interesting results are presented by abstract mathematical forms, which cannot be directly and effectively applied to the design of practical systems for industrial applications. In this paper, a relatively intuitional approach using Monodromy matrix is applied to investigate the system stability and design the advanced controller of interleaved boost converter. This Monodromy matrix contains all the comprehensive system information including the system parameters, external conditions, and coefficients of the controller [41, 42]. Accordingly, the influence of various parameters on overall system stability can be investigated intuitively and it is able to be used for the further study on interaction effect of the switching operation to system's behavior. Most importantly, the boundary conditions of stable operation and the information of stability margin and the parameters given can be obtained by the eigenvalues of this matrix. Furthermore, based on the knowledge gained from this matrix, a novel real-time cycle to cycle variable slope compensation method is proposed to stabilize the system, avoiding phenomena of subharmonic and chaotic operation. Theoretical analysis is validated numerically and experimentally to show the effectiveness of this proposed method.

The rest of this paper is organized as follows. The fundamental principle of the stability analysis methodology employed and the corresponding derivation of matrices is presented in Section II. The study of the control loop and the concept of control approach proposed is illustrated in Section III. Simulation results and the related analysis are shown in Section IV and the experimental results of interleaved boost converter using mixed-signal controller are given in Section V. The final section summarizes the conclusions drawn from investigation and analysis.

II. THEORETICAL PRINCIPLE AND MATRIX DERIVATION

A. Nonlinear phenomena

Nonlinear phenomena can commonly be found in the analysis of power electronics converters. Fig.1(a) shows experimental results of an interleaved boost converter (circuit parameters are shown in Table 1) when it is in the stable operation (period-1), in contrast, Fig.1(b) presents its chaotic operation where the only difference is a slight change at the values of slope compensation. Thus, the stability analysis is crucial to guarantee the stable operation of the converter as the small variation of parameters may change the performance of converter dramatically. The study of how the value of slope compensation affects the stability of the system and its influence to the margin of system stability can be fully given by using the Monodromy matrix based method which is presented in the following.

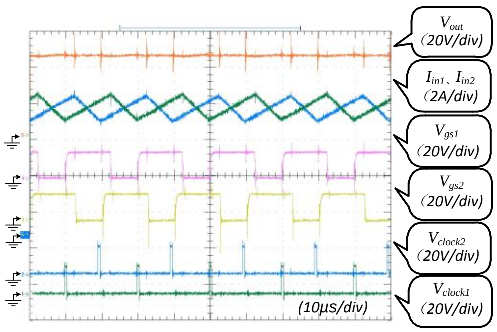

(a)

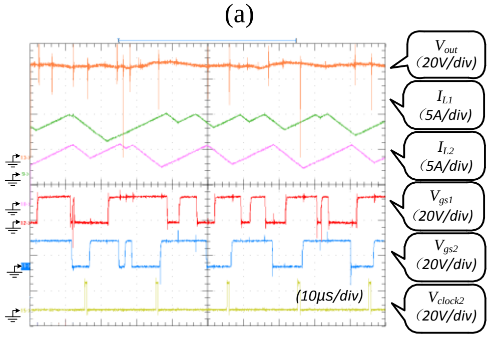

(b)

Fig.1 Operation of interleaved boost converter at two different values of slope compensation:
(a) Stable operation (period-1) (b) Chaotic operation

B. Concept of Monodromy Matrix Based Method

The topology of an interleaved boost converter and the diagram of a control strategy are shown in Fig.2, K_i and K_p represent the gains of the PI controller; K_{vc} and K_{il} are the gain of signals from the practical sampled output voltage v_c and inductor currents i_{Li} (i=1,2) to the controller respectively. The inductor currents i_{L1} , i_{L2}, capacitor voltage v_c and the output of the integrator in the feedback loop v_{ip} are chosen as the state variables. S_1 and S_2 are the switches employing the interleaving PWM control technique, which means that there is an 180-degree phase shift between them.

The key waveforms of the converter at different duty cycles in the steady state operation are illustrated in Fig.3(a) (when d>0.5) and Fig.3(b) (when d<0.5) respectively. It can be seen that there are four subintervals in one period for both operational modes and the state transition matrix can be represented as Φ_1~ Φ_4. The system states at different switching sequences can be described by the following state equations:

$$\dot{x} = \begin{cases} ①\mathbf{A}_1 x + \mathbf{B}_1 E & S_1 \text{ and } S_2 \text{ on} \\ ②\mathbf{A}_2 x + \mathbf{B}_2 E & S_1 \text{ on and } S_2 \text{ off} \\ ③\mathbf{A}_3 x + \mathbf{B}_3 E & S_1 \text{ off and } S_2 \text{ on} \\ ④\mathbf{A}_4 x + \mathbf{B}_4 E & S_1 \text{ and } S_2 \text{ off} \end{cases} \quad (1)$$

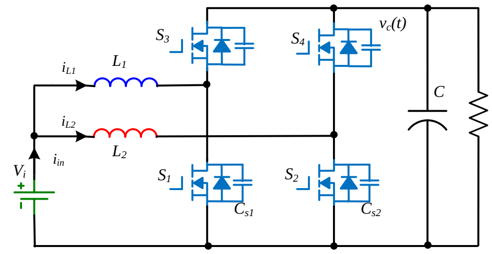

(a)

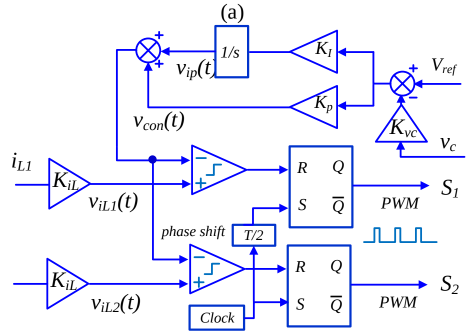

(b)

Fig.2 (a) Topology of interleaved boost converter
(b) Diagram of control strategy for interleaved boost converter

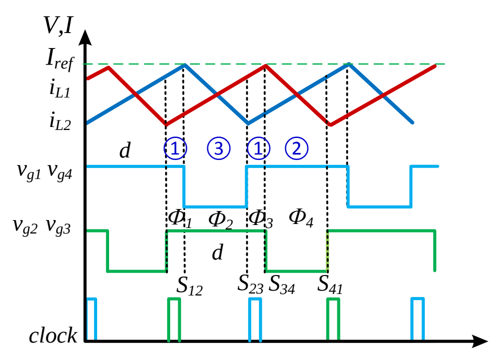

(a)

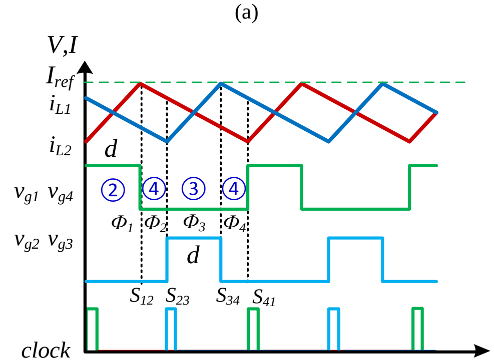

(b)

Fig.3 (a) Key operational waveforms in steady state (d>0.5)
(b) Key operational waveforms in steady state (d<0.5)

The concept of Monodromy matrix based method is to deduce the stability of a periodic solution by linearizing the system around the whole periodic orbit. This can be obtained by calculating the state transition matrices before and after each switching and the saltation matrix that describes the behaviors of the solution during switching. The derivation of this matrix is shown in Fig.4, which demonstrates perturbation evolves in one complete period through four different STM and four saltation matrices S in sequence.

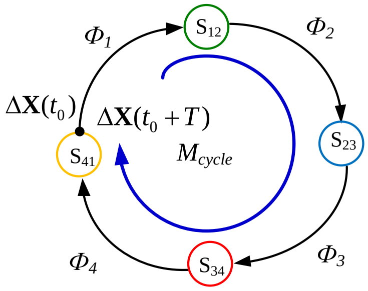

Fig.4 Diagram of derivation of Monodromy matrix

C. Theoretical Principle of Monodromy Matrix Based Method

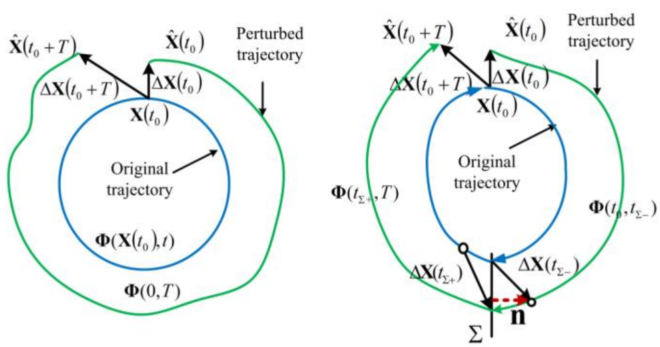

(a) (b)

Fig.5 Periodic solution and its perturbed solution

The fundamental theory of this method is presented in the following. As shown in Fig.5(a), assuming that a given system has an initial condition $\mathbf{x}(t_0)$ at time t_0 and it is perturbed to $\hat{\mathbf{x}}(t_0)$ such that the initial perturbation is $\Delta\mathbf{x}(t_0)=\mathbf{x}(t_0)-\hat{\mathbf{x}}(t_0)$. After the evolution of the original trajectory and the perturbed trajectory during time t, according to Floquet theory the perturbation at the end of the period can be related to the initial perturbation by

$$\Delta\mathbf{x}(t_0+T)=\mathbf{\Phi}\,\Delta\mathbf{x}(t_0) \tag{2}$$

where $\mathbf{\Phi}$ is called the state transition matrix (STM), which is a function of the initial state and time. For any power converter, the ON and OFF state of the switches makes the system to evolve through different linear time-invariant (LTI) subsystems, Therefore, for each subsystem, the STM can be obtained by the expression when the initial conditions are given.

$$\mathbf{\Phi}=e^{\mathbf{A}(t-t_0)} \tag{3}$$

where A is the state matrix that appears in the state equation:

$$\dot{\mathbf{x}}=\mathbf{Ax}+\mathbf{Bu} \tag{4}$$

In smooth systems, the fundamental matrix can be used to map the perturbation from the initial condition to the end of the period. Nevertheless, the vector field of a power electronics system is piecewise smooth and the vector field is discontinuous at the switching instant, which means that the STM cannot be utilized directly for stability analysis. As a result, some information representing the switching event needs to be introduced to fully describe the dynamic behavior of the system.

With the assumption that there is no jump in the state vector at switching instants, the Filippov method can be applied in the study of this discontinuous vector field, calculating the evolution of vectors during the interval of $[t_{\Sigma-}, t_{\Sigma+}]$. The principle of this approach is illustrated in Fig.5(b), and it describes the behaviour of a perturbation crossing the switching surface Σ. Assuming that there is an initial perturbation Δx(t0) at time of t_0, it then evolves to $\Delta x(t_{\Sigma-})$, starting to cross the switching manifold at time of $t_{\Sigma-}$. After time $(t_{\Sigma+}, t_{\Sigma-})$, it comes out of the switching surface and becomes $\Delta x(t_{\Sigma+})$. The saltation matrix **S** is used to map the perturbation before and after the switching manifold as follows [43].

$$\Delta\mathbf{x}(t_{\Sigma+})=\mathbf{S}\,\Delta\mathbf{x}(t_{\Sigma-}) \tag{5}$$

$$\mathbf{S}=\mathbf{I}+\frac{(f_{\Sigma+}-f_{\Sigma-})\mathbf{n}^T}{\mathbf{n}^T f_{\Sigma-}+\dfrac{\partial h}{\partial t}} \tag{6}$$

where **I** is the identity matrix of the same order of state variables; h contains information of the switching condition; **n** represents the normal vector to the switching surface; and $f_{\Sigma-}$ and $f_{\Sigma+}$ are the differential equations before and after the switching instant. The derivations of (5) and (6) have been presented in detail at the appendix. Hence the fundamental solution of a periodic system for one complete cycle, which is named the Monodromy matrix can be represented as follows:

$$\mathbf{M}=\Phi(t_0,t_0+T)=\Phi(t_{\Sigma+},t_0+T)\cdot\mathbf{S}\cdot\Phi(t_0,t_{\Sigma-}) \tag{7}$$

where $\Phi(t_0,t_{\Sigma-})$ and $\Phi(t_{\Sigma+},t_0+T)$ are the state transition matrices in the time intervals of $[t_0,t_{\Sigma-}]$ and $[t_{\Sigma-},t_0+T]$ respectively. The eigenvalues of the Monodromy matrix (also termed the Floquet multipliers) can be applied to predict the stability. If all the eigenvalues have magnitudes less than unity, the system will be stable, otherwise, the system will exhibit various bifurcation and chaotic behaviors determined by the movement trajectory of crossing the unit circle.

D. Matrix Derivation

In the operation of interleaved boost converter as shown in Fig.3, when the switches S_1 and S_2 are ON, the state equations can be expressed as:

$$\frac{dv_c}{dt}=-\frac{v_c}{RC},\ \frac{di_{L1}}{dt}=\frac{V_i}{L_1} \tag{8~9}$$

$$\frac{di_{L2}}{dt}=\frac{V_i}{L_2},\ \frac{dv_{ipi}}{dt}=K_I(K_{vc}v_c-V_{ref}) \tag{10~11}$$

When the switch S_1 is ON and S_2 is OFF, the state equations are:

$$\frac{dv_c}{dt}=\frac{i_{L2}R-v_c}{RC},\ \frac{di_{L1}}{dt}=\frac{V_i}{L_1} \tag{12~13}$$

$$\frac{di_{L2}}{dt}=\frac{V_i-v_c}{L_2},\ \frac{dv_{ip}}{dt}=K_I(K_{vc}v_c-V_{ref}) \tag{14~15}$$

When the switch S_1 is OFF and S_2 is ON, the state equations are:

$$\frac{dv_c}{dt}=\frac{i_{L1}R-v_c}{RC},\ \frac{di_{L1}}{dt}=\frac{V_i-v_c}{L_1} \qquad (16)\sim(17)$$

$$\frac{di_{L2}}{dt}=\frac{V_i}{L_2},\ \frac{dv_{ip}}{dt}=K_I(K_{vc}v_c-V_{ref}) \qquad (18)\sim(19)$$

When the switch S_1 and S_2 are OFF, the state equations are obtained as:

$$\frac{dv_c}{dt}=\frac{(i_{L1}+i_{L2})R-v_c}{RC},\ \frac{di_{L1}}{dt}=\frac{V_i-v_c}{L_1} \qquad (20)\sim(21)$$

$$\frac{di_{L2}}{dt}=\frac{V_i-v_c}{L_2},\ \frac{dv_{ipi}}{dt}=K_I(K_{vc}v_c-V_{ref}) \qquad (22)\sim(23)$$

The state equations above can be represented using vectors. Where x_1 is the capacitor voltage v_c, x_2 is the inductor current i_L, and x_3 the output of the integrator in the feedback loop v_{ip}, and the right-hand side state equations are expressed as:

$$f_1=\begin{bmatrix}-\frac{x_1}{RC}\\ \frac{V_i}{L_1}\\ \frac{V_i}{L_2}\\ K_I(K_{vc}x_1-V_{ref})\end{bmatrix}\ f_2=\begin{bmatrix}\frac{x_3R-x_1}{RC}\\ \frac{V_i}{L_1}\\ \frac{V_i-x_1}{L_2}\\ K_I(K_{vc}x_1-V_{ref})\end{bmatrix},$$

$$f_3=\begin{bmatrix}\frac{x_2R-x_1}{RC}\\ \frac{V_i-x_1}{L_1}\\ \frac{V_i}{L_2}\\ K_I(K_{vc}x_1-V_{ref})\end{bmatrix},\ f_4=\begin{bmatrix}\frac{(x_2+x_3)R-x_1}{RC}\\ \frac{V_i-x_1}{L_1}\\ \frac{V_i-x_1}{L_2}\\ K_I(K_{vc}x_1-V_{ref})\end{bmatrix} \qquad (24)$$

Thus, the corresponding state matrices for these four subintervals are shown in the following:

$$\mathbf{A}_1=\begin{bmatrix}-\frac{1}{RC}&0&0&0\\0&0&0&0\\0&0&0&0\\K_IK_{vc}&0&0&0\end{bmatrix},\ \mathbf{A}_2=\begin{bmatrix}-\frac{1}{RC}&0&\frac{1}{C}&0\\0&0&0&0\\-\frac{1}{L_2}&0&0&0\\K_IK_{vc}&0&0&0\end{bmatrix} \qquad (25)\sim(26)$$

$$\mathbf{A}_3=\begin{bmatrix}-\frac{1}{RC}&\frac{1}{C}&0&0\\-\frac{1}{L_1}&0&0&0\\0&0&0&0\\K_IK_{vc}&0&0&0\end{bmatrix},\ \mathbf{A}_4=\begin{bmatrix}-\frac{1}{RC}&\frac{1}{C}&\frac{1}{C}&0\\-\frac{1}{L_1}&0&0&0\\-\frac{1}{L_2}&0&0&0\\K_IK_{vc}&0&0&0\end{bmatrix} \qquad (27)\sim(28)$$

$$\mathbf{B_1}=\mathbf{B_2}=\mathbf{B_3}=\mathbf{B_4}=\begin{bmatrix}0&0&0&0\\0&0&\frac{1}{L_1}&0\\0&0&\frac{1}{L_2}&0\\0&0&0&-K_I\end{bmatrix},\ \mathbf{u}=\begin{bmatrix}0\\0\\V_i\\V_{ref}\end{bmatrix} \qquad (29)\sim(30)$$

According to the control strategy of peak current control, the switching transients occur at the beginning of each switching period and the moment when the value of inductor current i_{Li} equals the reference signal. Therefore, the switching conditions from the ON to OFF state can be expressed as $h_i(x,t)=0$ ($i=12,34$),where

$$h_i(x,t)=K_p(V_{ref}-K_{vc}v_c)+v_{ip}-K_{iL}i_{Li} \qquad (31)$$

Hence, its normal vector can be given by:

$$\mathbf{n}_{12}=\begin{bmatrix}\partial h_{12}/\partial x_1\\ \partial h_{12}/\partial x_2\\ \partial h_{12}/\partial x_3\\ \partial h_{12}/\partial x_4\end{bmatrix}=\begin{bmatrix}-K_pK_{vc}\\-K_{iL}\\0\\1\end{bmatrix} \qquad (32)$$

$$\mathbf{n}_{34}=\begin{bmatrix}\partial h_{34}/\partial x_1\\ \partial h_{34}/\partial x_2\\ \partial h_{34}/\partial x_3\\ \partial h_{34}/\partial x_4\end{bmatrix}=\begin{bmatrix}-K_pK_{vc}\\0\\-K_{iL}\\1\end{bmatrix} \qquad (33)$$

The saltation matrices $\mathbf{S_{23}}$ and $\mathbf{S_{41}}$ turn out to be identity matrices, since they are related to the switching event from the OFF state to the ON state for S_1 and S_2 at the initial instant of every clock cycle respectively, which means that the rising edge of the ramp causes the term of ∂h/∂t in (5) to be infinity. When the duty cycle d is bigger than 0.5, the system states evolve from the following sequence as illustrated in Fig.3(a):

①→③→①→②

Saltation matrix $\mathbf{S_{12a}}$ can be obtained as follows:

$$\mathbf{S}_{12a}=\begin{bmatrix}1-\frac{K_pK_{vc}x_3}{C(s_p+s_a)}&0&-\frac{K_{iL}x_3}{C(s_p+s_a)}&\frac{x_3}{C(s_p+s_a)}\\0&1&0&0\\ \frac{K_pK_{vc}x_1}{L_2(s_p+s_a)}&0&1+\frac{K_{iL}x_1}{L_2(s_p+s_a)}&-\frac{x_1}{L_2(s_p+s_a)}\\0&0&0&1\end{bmatrix} \qquad (34)$$

Similarly, the saltation matrix S34a can be derived as:

$$\mathbf{S}_{34a}=\begin{bmatrix}1-\frac{K_pK_{vc}x_2}{C(s_p+s_a)}&-\frac{K_{iL}x_2}{C(s_p+s_a)}&0&\frac{x_2}{C(s_p+s_a)}\\ \frac{K_pK_{vc}x_1}{L_1(s_p+s_a)}&1+\frac{K_{iL}x_1}{L_1(s_p+s_a)}&0&-\frac{x_1}{L_1(s_p+s_a)}\\0&0&1&0\\0&0&0&1\end{bmatrix} \qquad (35)$$

where

$$s_p=\mathbf{n}_{34}^T f_{on}=\mathbf{n}_{34}^T f_1=\frac{K_PK_{vc}x_1}{RC}-\frac{K_{iL}V_i}{L_2}+K_I(K_{vc}x_1-V_{ref}) \qquad (36)$$

$$s_a=\frac{\partial h}{\partial t}=0 \qquad (37)$$

For the interleaved control algorithm, the time of each subinterval can be represented in terms of d and T. The state transition matrices are given by the matrix exponential, hence

$$\begin{cases} \mathbf{\Phi}_1 = e^{\mathbf{A}_1(d-0.5)\mathrm{T}} \\ \mathbf{\Phi}_2 = e^{\mathbf{A}_3(1-d)\mathrm{T}} \\ \mathbf{\Phi}_3 = e^{\mathbf{A}_3(d-0.5)\mathrm{T}} \\ \mathbf{\Phi}_4 = e^{\mathbf{A}_2(1-d)\mathrm{T}} \end{cases} \tag{38}$$

When duty cycle d is less than 0.5, the evolution of system states can be expressed in the following sequence:

$$② \rightarrow ④ \rightarrow ③ \rightarrow ④$$

Fig.3(b) presents the key operational waveforms in steady state at this condition. The saltation matrices $\mathbf{S}_{12b}$ and $\mathbf{S}_{34b}$ can be calculated as follows:

$$\mathbf{S}_{12b} = \begin{bmatrix} 1-\dfrac{K_pK_{vc}x_2}{C(s_p+s_a)} & -\dfrac{K_{iL}x_2}{C(s_p+s_a)} & 0 & \dfrac{x_2}{C(s_p+s_a)} \\ \dfrac{K_pK_{vc}x_1}{L_1(s_p+s_a)} & 1+\dfrac{K_{iL}x_1}{L_1(s_p+s_a)} & 0 & -\dfrac{x_1}{L_1(s_p+s_a)} \\ 0 & 0 & 1 & 0 \\ 0 & 0 & 0 & 1 \end{bmatrix} \tag{39}$$

$$\mathbf{S}_{34b} = \begin{bmatrix} 1-\dfrac{K_pK_{vc}x_3}{C(s_p+s_a)} & 0 & -\dfrac{K_{iL}x_3}{C(s_p+s_a)} & \dfrac{x_3}{C(s_p+s_a)} \\ 0 & 1 & 0 & 0 \\ \dfrac{K_pK_{vc}x_1}{L_2(s_p+s_a)} & 0 & 1+\dfrac{K_{iL}x_1}{L_2(s_p+s_a)} & -\dfrac{x_1}{L_2(s_p+s_a)} \\ 0 & 0 & 0 & 1 \end{bmatrix} \tag{40}$$

where

$$s_p = \frac{-K_pK_{vc}(x_2R-x_1)}{RC} - \frac{K_{iL}V_i}{L_1} + K_I(V_{ref} - K_{vc}v_c) \tag{41}$$

$$s_a = \frac{\partial h}{\partial t} = 0 \tag{42}$$

When duty cycle is less than 0.5, the state transition matrices are given as

$$\begin{cases} \mathbf{\Phi}_1 = e^{\mathbf{A}_2 d\mathrm{T}} \\ \mathbf{\Phi}_2 = e^{\mathbf{A}_4(0.5-d)\mathrm{T}} \\ \mathbf{\Phi}_3 = e^{\mathbf{A}_3 d\mathrm{T}} \\ \mathbf{\Phi}_4 = e^{\mathbf{A}_4(0.5-d)\mathrm{T}} \end{cases} \tag{43}$$

Thus, the Monodromy matrix $\mathbf{M}$ can be calculated by the following expression:

$$\mathbf{M} = \mathbf{\Phi}_{cycle} = \mathbf{\Phi}_1 \times \mathbf{S}_{12} \times \mathbf{\Phi}_2 \times \mathbf{S}_{23} \times \mathbf{\Phi}_3 \times \mathbf{S}_{34} \times \mathbf{\Phi}_4 \times \mathbf{S}_{41} \tag{44}$$

This contains all of the information about the system input and load conditions, the parameters of the converter and the coefficients of the control loop, and therefore the influence of any system parameter on system stability can be analyzed using this matrix.

III. Proposed Control Method

Slope compensation is widely adopted in many different kinds of converters employing peak current mode control to avoid unstable phenomenon when the duty cycle d is bigger than 0.5. However, although several papers mentioned different methods to calculate the minimum required value of the compensation ramp in order to sufficiently eliminate subharmonic oscillations [44, 45], the influence of the slope parameter m_c to the margin of system stability cannot be investigated theoretically in these methods. In the Monodromy matrix based approach, the slope parameter m_c can be introduced in the derived saltation matrices $\mathbf{S}_{12}$ and $\mathbf{S}_{34}$. . Thus, the relationship among value of m_c, other variables and margin of stable operation can be intuitively demonstrated by using the locus of eigenvalues. Specifically, by altering various coefficients of the Monodromy matrix, the stability of the

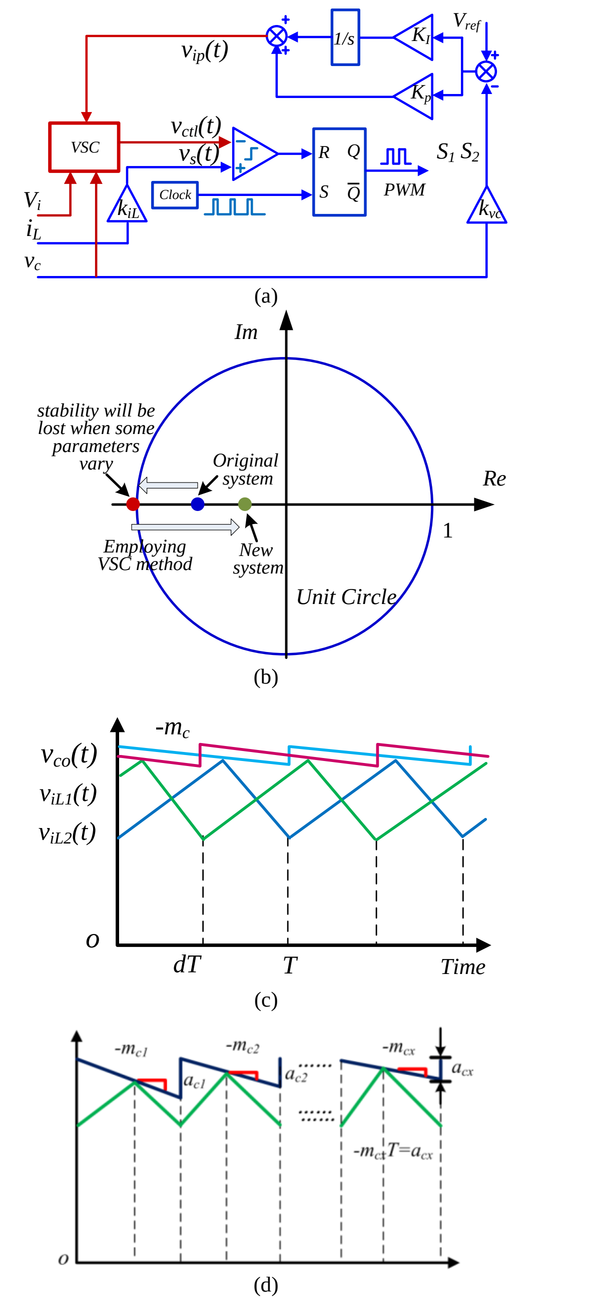

Fig.6 (a) Diagram of proposed control strategy
(b) Movement of eigenvalues applying proposed method
(c) Conventional constant slope compensation in interleaved boost converters
(d) Proposed real time variable slope compensation using Monodromy matrix

system will be influenced correspondingly. Based on this concept, a real time variable slope compensation method is proposed to control the nonlinear behavior of power converters, which is illustrated in Fig.6. The difference compared to conventional constant slope compensation is that the amplitude of compensation ramp a_c can be varying according to the change of external conditions, such as input and output voltage or load conditions.

When applying slope compensation to peak current control the time derivative of the switching manifold changes by adding a variable slope signal to the switching manifold h, thus the switching condition becomes

$$h_i(x,t) = K_p(V_{ref} - K_{vc}v_c) + v_{ip} + m_c t - K_{iL}i_{Li} \quad (45)$$

There is no effect on its normal vector, but compared to peak current control without slope compensation, the ∂h/∂t changes from 0 to the expression below:

$$\frac{\partial h}{\partial t} = m_c = -\frac{a_c}{T_s} \quad (46)$$

The diagram of proposed control strategy is shown in Fig.6(a), information of the input voltage V_i , output voltage v_c and the output of the PI controller are gathered as the input of the VSC control block. After the operation of calculation in this control block, a control signal $v_{ctrl}(t)$ containing the slope compensation with appropriate amplitude can be generated as the input signal of PWM generation block. As illustrated in Fig.6(b), the original system may lose the stability when some parameters are varying. Thus by choosing the appropriate parameter a_c in the new constructed Monodromy matrix, the corresponding eigenvalues can be located at any targeted places within the unit circle which indicates stable period-1 operation. In other words, for the given location of eigenvalues, the value of a_c can be calculated at every switching period accordingly, which is shown in Fig.6(d). The proposed method is to keep the magnitude of the eigenvalues the same at different input voltages. For the controller design, the relationship between the input voltage and required value of a_c must be obtained. Therefore, the following nonlinear transcendental equation should be solved numerically: $|eig(\mathbf{M}(0,T))| = R$. Where R is the radius of the circle on which the eigenvalues of the Monodromy matrix lie.

IV. SIMULATION RESULTS

The specifications of system parameters are presented in TABLE 1. Simulation results are produced based on the models built in Matlab/Simulink which using these parameters above. Fig. 7(a) shows the bifurcation diagram of output voltage v_c and inductor current i_{L1} at different input voltages. The input voltage is varied from 5 to 18 V with constant amplitude of slope (a_c=|m_c*T|=0.1). It can be seen that the system experiences from chaotic state to double period (period-2) and eventually to stable period-1 operation with the increase of input voltages. The bifurcation phenomena take places when the input is set close to 8.75V, where the system changes between double-period oscillation and period-1 operation. The corresponding eigenvalues of system at different inputs can be calculated using the expression of Monodromy matrix derived and the movement track of eigenvalues at different inputs can be plotted as shown in Fig. 7(b). The related eigenvalues reach the border of unit circle when input voltage equals 8.75V, which demonstrates the system will exhibit period doubling oscillation at this condition. The numerical computation matches with the simulation results well and the margin of system stability can be intuitively indicated by the locus of eigenvalues.

TABLE 1
SPECIFICATIONS OF SYSTEM PARAMETERS

Parameters	Value	Parameters	Value
Input voltage （V）	5~18,	Frequency （kHz）	50
Output voltage （V）	24,	K_{iL}	1/8.5
Power rating （W）	60	K_{p1}	0.5
Inductance （μH）	75	K_{i1}	2000
Output capacitance (μF)	40	m_c*T	-0.10
K_{vc}	1/10		

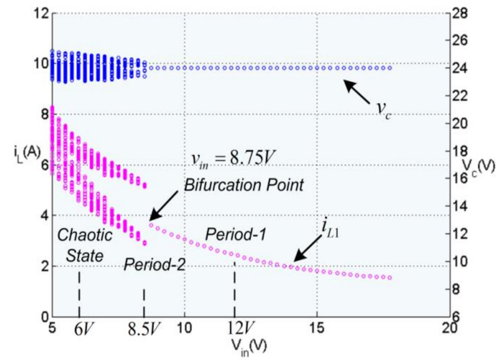

(a)

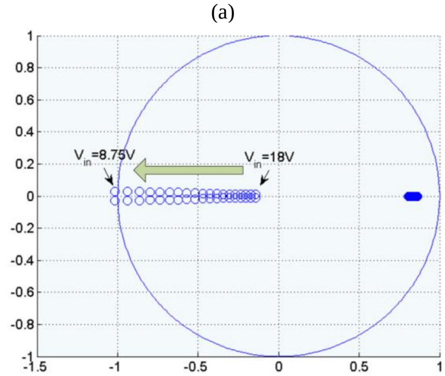

(b)

Fig. 7(a) Bifurcation diagram of output voltage and inductor current at different input voltages
(b) corresponding locus of eigenvalues

Key operational waveforms and FFT spectrum at different inputs (12V, 8.5V and 6 V) are shown in Fig.8(a), (b) and (c) respectively. The waveforms are output voltage v_c, inductor current of one phase i_{L1}, corresponding control signal i_{ctrl}, generated PWM drive signal and FFT spectrum of drive signal from top to bottom. When input voltage equals 12V, the system is to run at stable period 1, which is the expected operation region as shown in Fig.7(a). When the input voltage is reduced to 8.5V, the frequency of generate PWM reduces from 50kHz to 25kHz according to the FFT spectrum. The non-periodic and random-like waveforms demonstrate that the converter is to run at chaotic operation. We can see the ripple of voltage and current increase dramatically from period-1 to the chaotic operation through period 2. Specifically, the ripple voltage changes from nearly 0.05V to 1.7V and ripple current varies from 1.5A to 3.2A. Thus it is evident that the chaotic operation does cause more losses and degrade the performance of the converter.

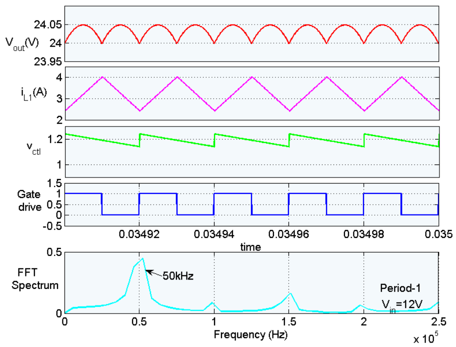

(a)

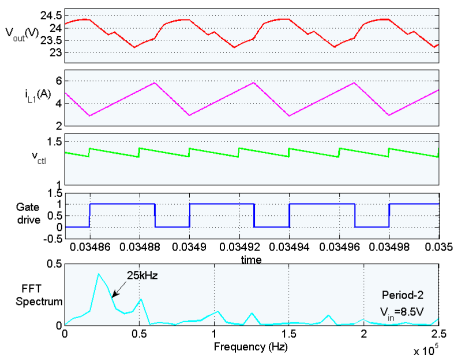

(b)

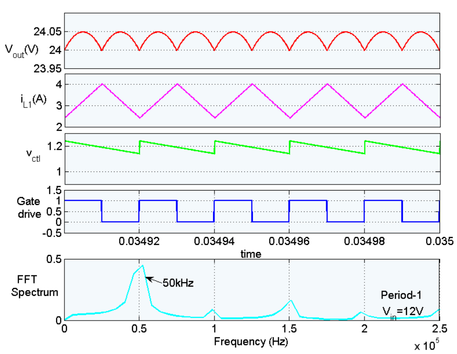

Fig.8 Key operational waveforms and FFT spectrum at different operation states in simulation:
(a) period-1 (b) period-2 (c) chaotic state

In order to further study the relationship among V_{in}, a_c and system stability, the bifurcation diagram of inductor current and output voltage at different input voltages and a_c are shown in Fig.9. The amplitude of slope is set at 0.05 to 0.20 with the step of 0.05 and the bifurcation points varies from 10.5V to 5.5V input when a_c is changed from 0.05 to 0.20 accordingly. It clearly shows the bifurcation points vary at different a_c, exhibiting certain linear relationship. The figure also shows that bigger amplitude of slope compensation brings in the wider range of stable operation at the same given input conditions. The Monodromy matrix can be expressed as a function **M** in terms of a_c and V_{in}:

$$\mathbf{M} = M(a_c, V_{in}) \tag{47}$$

The border value of the stable operating region can be calculated using the Monodromy matrix derived, which provides the design guidance for the given system.

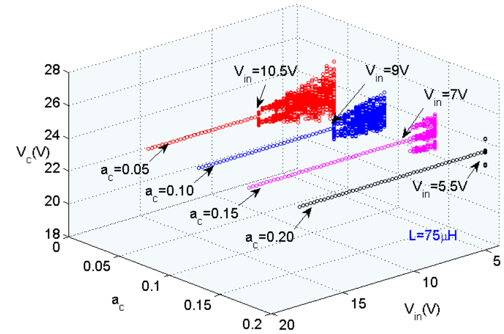

(a)

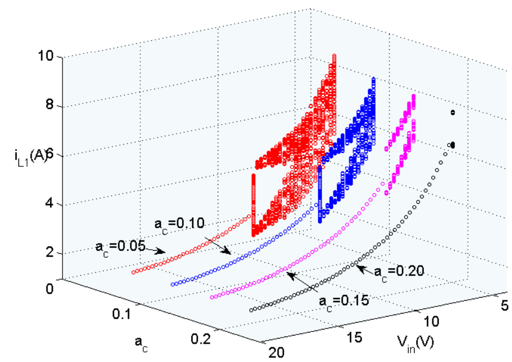

(b)

Fig.9 Bifurcation diagram of inductor current and output voltage at different input voltages and a_c in Simulation:
(a) Output voltage (b) Inductor current

V. EXPERIMENTAL VERIFICATION

A. *Bifurcation Diagram*

To verify the analysis on simulation results, an interleaved boost converter with relevant control circuit have been designed using the specification presented in Table 1. Fig.10 presents the experimental bifurcation diagram of output voltage and inductor current at the conditions of different input voltages and values of a_c. Graphs are reconstructed based on the sampled and stored data, which are from the generated file by using Labview. Compared with the shown in Fig.9, it can be seen that both waveforms are quite close but with some differences in terms of the practical values of a_c employed, profile and bifurcation point. The practical required value of a_c is slightly bigger (about 0.05) than the ones set in the simulation. Other differences are caused by the varying steps of input voltage in the experiment and the constant step setting in the simulation. The simulation results are from the ideal model-based calculation, and thus the sampled points generated for constant values are exactly located at one point. In contrast, errors in the experimental results are caused by the sampling resolution and quantization effect, and thus the constant values to sample will be transferred as values with some errors in the DSP controller. The errors are also related to settings of the zero-order hold and capture window in relevant registers, and this is normally set within a certain acceptable range to guarantee accuracy. In general, the simulation results are reliable enough so as to be used to facilitate the practical circuit design.

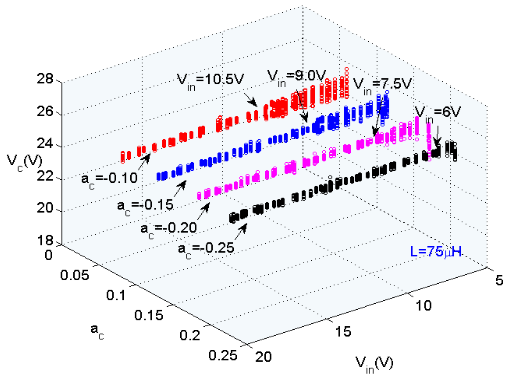

(a)

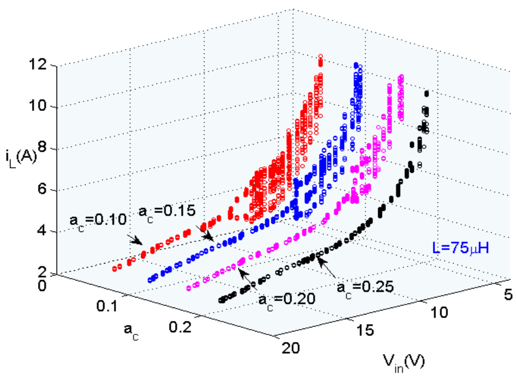

(b)

Fig.10 Experimental bifurcation diagram of inductor current and output voltage at different input voltages and m_c: (a) output voltage (b) inductor current

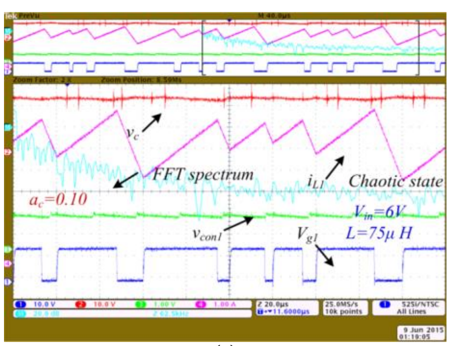

(a)

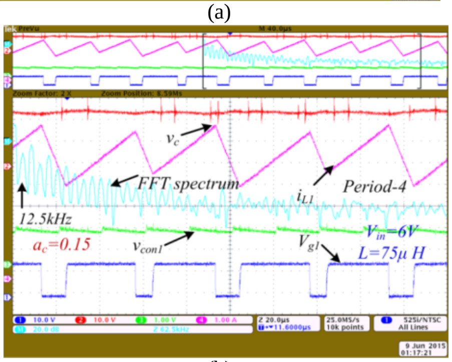

(b)

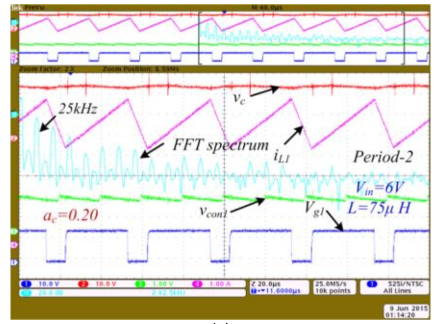

(c)

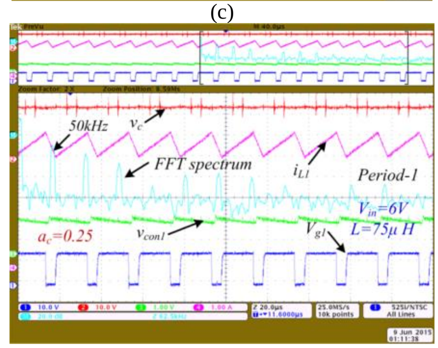

(d)

Fig.11 Experimental results of key operational waveforms at different compensation slope
(a) a_c=0.10 (b) a_c=0.15 (c) a_c=0.20 (d) a_c=0.25

The influence of different value of a_c to the operation of converter is demonstrated in Fig.11. The input voltage is set at 6V, and a_c is set from 0.1, to 0.25 with the step of 0.05. Fig.11(a) shows the converter is operated in the chaotic state when a_c equals 0.1; when the a_c is changed to 0.15, the FFT spectrum curve indicates the converter is in the operation of period-4, with the fundamental frequency of 12.5kHz, which is a quarter of period-1. The operation of converter becomes to period-2 when a_c is set to 0.20, and stable operation of period-1 will occur if a_c is increased to 0.25. The key operation waveforms are presented in Fig.11 (b), (c) and (d) respectively. It is evident that the values of compensation ramp affect dramatically to the stability of converter's operation and the larger value of a_c can increase the stability of system.

B. Real-Time Cycle-to-Cycle Variable Slope Compensation Control

In order to control nonlinear behavior and improve the performance of converters, an approach named real-time cycle-by-cycle variable slope compensation (VSC) is proposed in this section, which is based on the knowledge of Monodromy matrix. The concept and principles of this method are presented in section III, but the challenge is the practical implantation of variable slope compensation. To address this problem, a high-performance Digital to Analogue (DAC) is employed with a DSP controller to achieve this advanced control method. As illustrated in Fig.12(a), a TI F28335 based-DSP controller is used as the core processor to achieve the functions of voltage signal sampling, calculation of control strategy and sending commands to the external high-speed waveform generator AD9106 to produce the control signals. Two continuous time inductor currents are sampled and scaled by current sensors, and corresponding signals are fed into the comparators to generate the PWM signals. Fig.13 (b) presents the operational waveforms of control and clock signals, the upper waveforms are two current references added by variable slope compensations with a 180 degree shift, which are generated by this programmable DAC, and the bottom waveforms are the corresponding clock signals. The amplitudes of the slopes are programmed to increase within a given step to demonstrate the capability of cycle-by-cycle slope control.

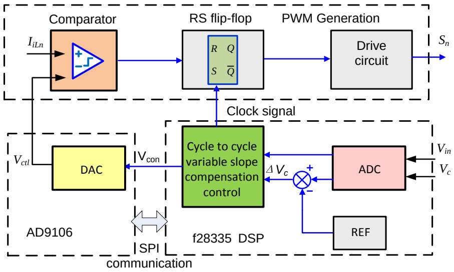

(a)

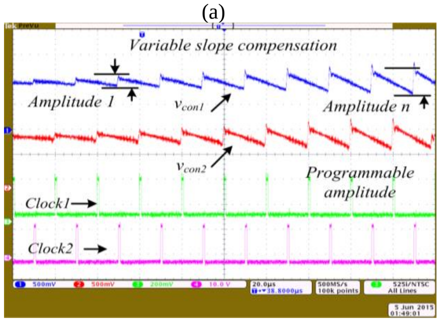

(b)

Fig.12 Implementation of variable slope compensation control:
(a) Control strategy in the practical circuit (b) control and clock signals

As discussed in Section III, the eigenvalues of Monodromy matrix can be used to predict the bifurcation points of the system and the locus of eigenvalues can indicate the margin of the stable range at different levels of variation in system parameters or external input and output conditions. In other words, if a specific margin is set, the corresponding compensation slope can be calculated by the given parameters. Here, if the eigenvalues are placed at the radius of 0.5 in the unit circle, for example, the following nonlinear transcendental equation can be obtained which should be solved numerically:

$$|eig(\mathbf{M}(0,T))| = 0.5 \tag{48}$$

The relationship of input voltage and the required mc can be given in the form of a third order polynomial expression:

$$m_c \cdot T = -2.098\times10^{-5}\times V_{in}^3 + 7.832\times10^{-4}\times V_{in}^2 + 5.5\times10^{-3}\times V_{in} - 0.2561 \tag{49}$$

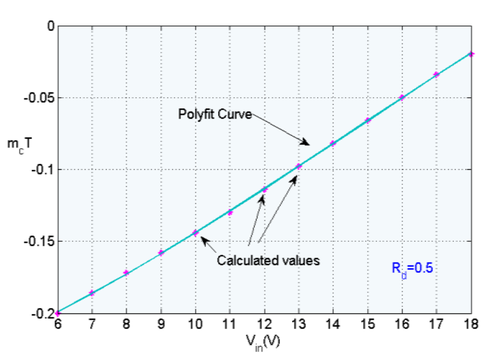

Fig.13 Polyfit curve and calculated values of m_c vs. input voltage

Fig.13 shows the polynomial fitting curve and the calculated values of m_c at different input voltages for the given radius of 0.5. Thus, in digital VSC, the amplitudes of the compensation ramp are calculated from the input voltages according to the expression above.

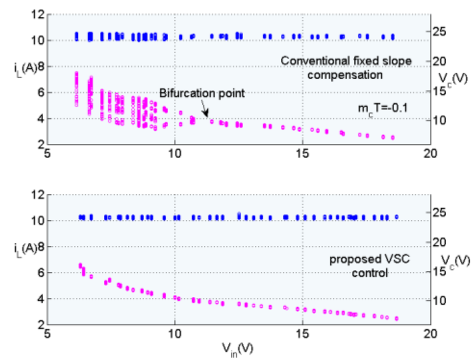

(a)

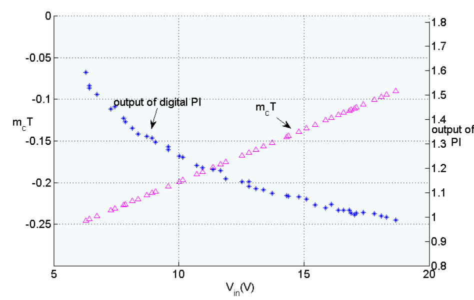

(b)

Fig.14 (a) Comparison of conventional fixed slope compensation and proposed method
(b) calculated values of m_c and output of PI in digital controller

A comparison of conventional fixed slope compensation and the proposed method under digital control is presented in Fig.14(a). It can be seen that bifurcation occurs when the input voltage is around 11 volts with conventional fixed slope compensation; in contrast, the converter remains stable over the whole range of input voltage from 6 to 18 volts when employing VCS. Thus the range of stable operation is effectively extended by using the proposed method. Fig.14(b) demonstrates the calculated values of m_c*T and the output of digital PI in the operation at different input voltages, which shows that with a linear increase in the absolute value of m_c*T, the output of digital PI falls inversely.

Fig.15 presents the effect of the proposed method on the control of nonlinearity in converters. The waveforms of the output voltage, inductor current, feedback control signals and gate drives are displaoyed from the top to the bottom. Fig.15 (a) and (b) respectively show the moments where the converter loses stability from stable operation of period-1 to the chaotic state and to the period-2. By employing VSC, the system can be kept in stable operation at certain operating conditions; in contrast, when the controller is switched to use conventional fixed slope control, the converter loses stability immediately at one cycle time. Similarly, the system can regain stability by switching to the proposed method within a few time periods of switching cycles. Compared to the stable state, it can also be seen that the ripples of output voltage and inductor current increase remarkably when the converter is in the unstable chaotic state.

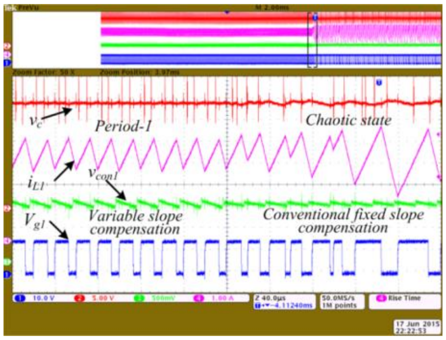

(a)

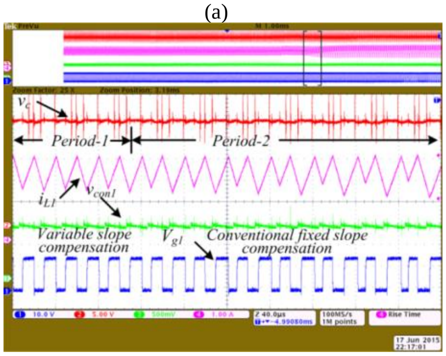

(b)

Fig.15 Control of nonlinearity in converters by employing cycle by cycle variable slope compensation:
(a) period-1 to chaotic state; (b) period-1 to period-2

VI. Conclusion

The nonlinear phenomenon for an interleaved boost converter is discussed and a new control method based on Monodromy matrix has been presented in this paper. The system dynamic behavior dependent stability and further understanding of the tipping point for unstable operations can be gained by employing this adopted nonlinear analysis method. This method can be readily extended to other types of DC-DC converters using interleaving structure. In addition, it provides a new perspective on control laws of designing the appropriate controllers to address the nonlinearities in DC-DC converters. Accordingly, a real time slope compensation method is proposed to mitigate the nonlinear behavior, which is successfully to extend the range of stable operation and effectively to increase the dynamic robustness by control the nonlinearity as validated by experimental results.

Appendix

The theory of Filippov provides a generalized definition of system solutions with switching behavior [17, 43, 46]. Such systems can be described as:

$$\dot{\mathbf{x}}(t)=\begin{cases} f_{-}(\mathbf{x}(t),t) & \mathbf{x}\in V_{-} \\ f_{\Sigma}(\mathbf{x}(t),t) & \mathbf{x}\in \Sigma \\ f_{+}(\mathbf{x}(t),t) & \mathbf{x}\in V_{+} \end{cases} \tag{A1.1}$$

where $f_{-}(\mathbf{x}(t),t)$ and $f_{+}(\mathbf{x}(t),t)$ represent the smooth vector fields before and after switching respectively. V- and V+ are two different regions in state space and the switching manifold Σ separates them as shown in Figure A1.1

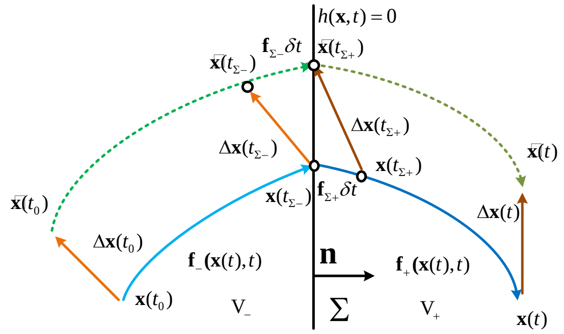

Fig.A1.1 Solution of nonsmooth system and its perturbed solution

In smooth systems, the evaluation of perturbation from the initial condition to the end of the period can be mapped by the fundamental matrix. In non-smooth systems, however, the switching instant makes the vector field discontinuous. As a result, the fundamental matrix breaks down and the information of the switching instant needs to be taken into account. The relations of perturbation vectors $\Delta\mathbf{x}(t_{\Sigma-})$ and $\Delta\mathbf{x}(t_{\Sigma+})$ which are before and after the switching respectively, can be described using the saltation matrix

$$\Delta\mathbf{x}(t_{\Sigma+})=\mathbf{S}\ \Delta\mathbf{x}(t_{\Sigma-}) \tag{A1.2}$$

The following equations can be obtained:

$$\begin{cases} \Delta\mathbf{x}(t_0)=\tilde{\mathbf{x}}(t_0)-\mathbf{x}(t_0) \\ \Delta\mathbf{x}(t)=\tilde{\mathbf{x}}(t)-\mathbf{x}(t) \\ \tilde{\mathbf{x}}(t_{\Sigma-})=\mathbf{x}(t_{\Sigma-})+\Delta\mathbf{x}(t_{\Sigma-}) \\ \tilde{\mathbf{x}}(t_{\Sigma+})=\mathbf{x}(t_{\Sigma+})+\Delta\mathbf{x}(t_{\Sigma+}) \\ t_{\Sigma+}=t_{\Sigma-}+\delta t \end{cases} \tag{A1.3}$$

δt represents the time difference before and after the switching instant, which is small enough. By employing Taylor series expansion, the relationship of the state vectors can be expressed as follows:

$$\tilde{\mathbf{x}}(t_{\Sigma+})=\tilde{\mathbf{x}}(t_{\Sigma-}+\delta t)=\tilde{\mathbf{x}}(t_{\Sigma-})+f_{\Sigma-}\delta t \tag{A1.4}$$

$$\mathbf{x}(t_{\Sigma+})=\mathbf{x}(t_{\Sigma-}+\delta t)=\mathbf{x}(t_{\Sigma-})+f_{\Sigma+}\delta t \tag{A1.5}$$

By substituting (A1.4), (A1.5) into (A1.3), the following is obtained:

$$\begin{aligned}\Delta\mathbf{x}(t_{\Sigma+})&=\tilde{\mathbf{x}}(t_{\Sigma+})-\mathbf{x}(t_{\Sigma+})=\tilde{\mathbf{x}}(t_{\Sigma-})-\mathbf{x}(t_{\Sigma-})+(f_{\Sigma-}-f_{\Sigma+})\delta t \\ &=\Delta\mathbf{x}(t_{\Sigma-})+(f_{\Sigma-}-f_{\Sigma+})\delta t\end{aligned} \tag{A1.6}$$

Switching conditions satisfy the following relationship:

$$\begin{cases} h(\mathbf{x}(t_{\Sigma-}),t_{\Sigma-})=0 \\ h(\mathbf{x}(t_{\Sigma+}),t_{\Sigma+})=0 \end{cases} \tag{A1.7}$$

Also using the Taylor series expansion on h(x(t),t), an expression can be derived in terms of δt:

$$\begin{aligned} h(\tilde{\mathbf{x}}(t_{\Sigma+}),t_{\Sigma+})&=h(\mathbf{x}(t_{\Sigma-})+\Delta\mathbf{x}(t_{\Sigma-})+f_{\Sigma-}\delta t,t_{\Sigma-}+\delta t) \\ &=\underbrace{h(\mathbf{x}(t_{\Sigma-}),t_{\Sigma-})}_{0}+\mathrm{m}\,\delta t+\mathbf{n}^{T}(\Delta\mathbf{x}(t_{\Sigma-})+f_{\Sigma-}\delta t)=0 \end{aligned} \tag{A1.8}$$

where:

$$\mathbf{n}=\frac{\partial h}{\partial \mathbf{x}}\bigg|_{(t_{\Sigma},\mathbf{x}(t_{\Sigma}))} \tag{A1.9}$$

and:

$$m = \frac{\partial h(\mathbf{x}(t_{\Sigma-}), t_{\Sigma-})}{\partial t} = \frac{\partial h(\mathbf{x}(dT), dT)}{\partial t} = \frac{\partial h}{\partial t}\Big|_{x(\mathrm{dT}),\mathrm{dT}} \quad \text{(A1.10)}$$

Here, **n** represents the normal to the switching manifold. The expression for δt can be obtained as:

$$\delta t = -\frac{\mathbf{n}^T \Delta\mathbf{x}(t_{\Sigma-})}{\mathbf{n}^T f_{\Sigma-} + m} \quad \text{(A1.11)}$$

Substituting (A1.8), (A1.9) and (A1.10) into (A1.11), the relationship between the perturbations vectors before and after the switching is shown as follows:

$$\Delta\mathbf{x}(t_{\Sigma+}) = \Delta\mathbf{x}(t_{\Sigma-}) + (f_{\Sigma+} - f_{\Sigma-})\frac{\mathbf{n}^T \Delta\mathbf{x}(t_{\Sigma-})}{\mathbf{n}^T f_{\Sigma-} + m} \quad \text{(A1.12)}$$

Comparing (A1.2) and (A1.12), the saltation matrix can be written as:

$$\mathbf{S} = \mathbf{I} + \frac{(f_{\Sigma+} - f_{\Sigma-})\mathbf{n}^T}{\mathbf{n}^T f_{\Sigma-} + \dfrac{\partial h}{\partial t}} \quad \text{(A1.13)}$$

REFERENCES

[1] T. Jiun-Ren, W. Tsai-Fu, W. Chang-Yu, C. Yaow-Ming, and L. Ming-Chuan, "Interleaving Phase Shifters for Critical-Mode Boost PFC," *Power Electronics, IEEE Transactions on,* vol. 23, pp. 1348-1357, 2008.

[2] L. Wuhua and H. Xiangning, "A Family of Isolated Interleaved Boost and Buck Converters With Winding-Cross-Coupled Inductors," *Power Electronics, IEEE Transactions on,* vol. 23, pp. 3164-3173, 2008.

[3] K. Dong-Hee, C. Gyu-Yeong, and L. Byoung-Kuk, "DCM Analysis and Inductance Design Method of Interleaved Boost Converters," *Power Electronics, IEEE Transactions on*, vol. 28, pp. 4700-4711, 2013.

[4] O. Hegazy, J. Van Mierlo, and P. Lataire, "Analysis, Modeling, and Implementation of a Multidevice Interleaved DC/DC Converter for Fuel Cell Hybrid Electric Vehicles," *Power Electronics, IEEE Transactions on,* vol. 27, pp. 4445-4458, 2012.

[5] J. Doo-Yong, J. Young-Hyok, P. Sang-Hoon, J. Yong-Chae, and W. Chung-Yuen, "Interleaved Soft-Switching Boost Converter for Photovoltaic Power-Generation System," *Power Electronics, IEEE Transactions on*, vol. 26, pp. 1137-1145, 2011.

[6] N. Long-xian, S. Kai, Z. Li, X. Yan, C. Min, and L. Rosendahl, "A power conditioning system for thermoelectric generator based on interleaved Boost converter with MPPT control," in *Electrical Machines and Systems (ICEMS), 2011 International Conference on*, 2011, pp. 1-6.

[7] Y. Chen, C. K. Tse, S. C. Wong, and S. S. Qiu, "Interaction of fast-scale and slow-scale bifurcations in current-mode controlled dc/dc converters," *International Journal of Bifurcation and Chaos,* vol. 17, pp. 1609-1622, May 2007.

[8] D. Giaouris, S. Banerjee, O. Imrayed, K. Mandal, B. Zahawi, and V. Pickert, "Complex Interaction Between Tori and Onset of Three-Frequency Quasi-Periodicity in a Current Mode Controlled Boost Converter," *IEEE Transactions on Circuits and Systems I-Regular Papers,* vol. 59, pp. 207-214, Jan 2012.

[9] H. H. C. Lu and C. K. Tse, "Study of low-frequency bifurcation phenomena of a parallel-connected boost converter system via simple averaged models," *IEEE Transactions on Circuits and Systems I-Fundamental Theory and Applications,* vol. 50, pp. 679-686, May 2003.

[10] P. T. Krein, J. Bentsman, R. M. Bass, and B. C. Lesieutre, "On the use of averaging for the analysis of power electronic systems," *IEEE Transactions on Power Electronics* , vol. 5, pp. 182-190, 1990.

[11] B. Lehman and R. M. Bass, "Switching frequency dependent averaged models for PWM DC-DC converters," *IEEE Transactions on Power Electronics,* vol. 11, pp. 89-98, 1996.

[12] V. A. Caliskan, G. C. Verghese, and A. M. Stankovic, "Multifrequency averaging of DC/DC converters," *IEEE Transactions on Power Electronics,* vol. 14, pp. 124-133, Jan 1999.

[13] S. R. Sanders, J. M. Noworolski, X. Z. Liu, and G. C. Verghese, "Generalized averaging method for power conversion circuits," *IEEE Transactions on Power Electronics,* vol. 6, pp. 251-259, 1991.

[14] S. Jian and R. M. Bass, "A new approach to averaged modeling of PWM converters with current-mode control," in *Industrial Electronics, Control and Instrumentation, 1997. IECON 97. 23rd International Conference on*, 1997, pp. 599-604 vol.2.

[15] M. di Bernardo and F. Vasca, "Discrete-time maps for the analysis of bifurcations and chaos in DC/DC converters," *IEEE Transactions on Circuits and Systems I-Regular Papers,* vol. 47, pp. 130-143, Feb 2000.

[16] S. Almer, U. Jonsson, C. Y. Kao, and J. Mari, "Global stability analysis of DC-DC converters using sampled-data modeling," *Proceedings of the 2004 American Control Conference, Vols 1-6,* pp. 4549-4554, 2004.

[17] D. Giaouris, S. Banerjee, B. Zahawi, and V. Pickert, "Stability Analysis of the Continuous-Conduction-Mode Buck Converter Via Filippov's Method," *IEEE Transactions on Circuits and Systems I: Regular Papers,* vol. 55, pp. 1084-1096, 2008.

[18] S. K. Mazumder and K. Acharya, "Multiple Lyapunov Function Based Reaching Condition for Orbital Existence of Switching Power Converters," *IEEE Transactions on Power Electronics,* vol. 23, pp. 1449-1471, 2008.

[19] I. A. Hiskens and M. A. Pai, "Trajectory sensitivity analysis of hybrid systems," *IEEE Transactions on Circuits and Systems I-Regular Papers,* vol. 47, pp. 204-220, Feb 2000.

[20] E. Rodriguez, A. El Aroudi, F. Guinjoan, and E. Alarcon, "A Ripple-Based Design-Oriented Approach for Predicting Fast-Scale Instability in DC-DC Switching Power Supplies," *IEEE Transactions on Circuits and Systems I-Regular Papers,* vol. 59, pp. 215-227, Jan 2012.

[21] A. El Aroudi, E. Rodriguez, R. Leyva, and E. Alarcon, "A Design-Oriented Combined Approach for Bifurcation Prediction in Switched-Mode Power Converters," *IEEE Transactions on Circuits and Systems II-Express Briefs,* vol. 57, pp. 218-222, Mar 2010.

[22] K. Mehran, D. Giaouris, and B. Zahawi, "Stability Analysis and Control of Nonlinear Phenomena in Boost Converters Using Model-Based Takagi-Sugeno Fuzzy Approach," *IEEE Transactions on Circuits and Systems I-Regular Papers,* vol. 57, pp. 200-212, Jan 2010.

[23] K. H. Wong, "Output capacitor stability study on a voltage-mode buck regulator using system-poles approach," *IEEE Transactions on Circuits and Systems Ii-Express Briefs,* vol. 51, pp. 436-441, Aug 2004.

[24] X. M. Wang, B. Zhang, and D. Y. Qiu, "The Quantitative Characterization of Symbolic Series of a Boost Converter," *IEEE Transactions on Power Electronics,* vol. 26, pp. 2101-2105, Aug 2011.

[25] N. Quanmin, J. Zhizhong, Q. Chengchao, and W. Hengli, "Study on Bifurcation and Chaos in Boost Converter Based on Energy Balance Model," in *Power and Energy Engineering Conference, 2009. APPEEC 2009. Asia-Pacific*, 2009, pp. 1-5.

[26] A. El Aroudi, D. Giaouris, H. Ho-Ching Iu, and I. A. Hiskens, "A Review on Stability Analysis Methods for Switching Mode Power Converters," *IEEE Journal on Emerging and Selected Topics in Circuits and Systems,* vol. 5, pp. 302-315, 2015.

[27] E. Ott, C. Grebogi, and J. A. Yorke, "Controlling chaos," *Physical review letters,* vol. 64, p. 1196, 1990.

[28] R. S. Bueno and J. L. R. Marrero, "Application of the OGY method to the control of chaotic DC-DC converters: Theory and experiments," *Iscas 2000: IEEE International Symposium on Circuits and Systems - Proceedings, Vol Ii,* pp. 369-372, 2000.

[29] A. Y. Goharrizi, A. Khaki-Sedigh, and N. Sepehri, "Observer-based adaptive control of chaos in nonlinear discrete-time systems using time-delayed state feedback," *Chaos Solitons & Fractals,* vol. 41, pp. 2448-2455, Sep 15 2009.

[30] N. Wang, G. N. Lu, X. Z. Peng, and Y. K. Cai, "A Research on Time Delay Feedback Control Performance in Chaotic System of Dc-Dc Inverter," *2013 IEEE International Conference on Vehicular Electronics and Safety (Icves),* pp. 215-218, 2013.

[31] W. Ma, M. Y. Wang, S. X. Liu, S. Li, and P. Yu, "Stabilizing the Average-Current-Mode-Controlled Boost PFC Converter via Washout-Filter-Aided Method," *IEEE Transactions on Circuits and Systems Ii-Express Briefs,* vol. 58, pp. 595-599, Sep 2011.

[32] A. El Aroudi, R. Haroun, A. Cid-Pastor, and L. Martinez-Salamero, "Suppression of Line Frequency Instabilities in PFC AC-DC Power Supplies by Feedback Notch Filtering the Pre-Regulator Output Voltage," *IEEE Transactions on Circuits and Systems I: Regular Papers,* vol. 60, pp. 796-809, 2013.

[33] L. Wei-Guo, Z. Luo-Wei, and W. Jun-Ke, "Self-Stable Chaos Control of dc—dc Converter," *Chinese Physics Letters,* vol. 26, p. 030503, 2009.

[34] J. Xu, G. Zhou, and M. He, "Improved digital peak voltage predictive control for switching DC–DC converters," *IEEE Transactions on Industrial Electronics,* vol. 56, pp. 3222-3229, 2009.
[35] E. Rodriguez, E. Alarcon, H. H. C. Iu, and A. El Aroudi, "A Frequency Domain Approach for Controlling Chaos in Switching Converters," *2010 IEEE International Symposium on Circuits and Systems,* pp. 2928-2931, 2010.
[36] Y. F. Zhou, H. H. C. Iu, C. K. Tse, and J. N. Chen, "Controlling chaos in DC/DC converters using optimal resonant parametric perturbation," *2005 IEEE International Symposium on Circuits and Systems (Iscas), Vols 1-6, Conference Proceedings,* pp. 2481-2484, 2005.
[37] Y. Zhou, C. K. Tse, S.-S. Qiu, and F. C. M. Lau, "Applying resonant parametric perturbation to control chaos in the buck dc/dc converter with phase shift and frequency mismatch considerations," *International Journal of Bifurcation and Chaos,* vol. 13, pp. 3459-3471, 2003.
[38] B. Bocheng, Z. Guohua, X. Jianping, and L. Zhong, "Unified Classification of Operation-State Regions for Switching Converters with Ramp Compensation," *IEEE Transactions on Power Electronics,* vol. 26, pp. 1968-1975, 2011.
[39] N. Inaba, T. Endo, T. Yoshinaga, and K. Fujimoto, "Collapse of mixed-mode oscillations and chaos in the extended Bonhoeffer-van Der pol oscillator under weak periodic perturbation," in *Circuit Theory and Design (ECCTD), 2011 20th European Conference on*, 2011, pp. 369-372.
[40] K. Guesmi, A. Hamzaoui, and J. Zaytoon, "Control of nonlinear phenomena in DC–DC converters: Fuzzy logic approach," *International Journal of Circuit Theory and Applications,* vol. 36, pp. 857-874, 2008.
[41] H. Wu, V. Pickert, and D. Giaouris, "Nonlinear analysis for interleaved boost converters based on Monodromy matrix," in *Energy Conversion Congress and Exposition (ECCE), 2014 IEEE,* 2014, pp. 2511-2516.
[42] H. Wu and V. Pickert, "Stability analysis and control of nonlinear phenomena in bidirectional boost converter based on the Monodromy matrix," in *Applied Power Electronics Conference and Exposition (APEC), 2014 Twenty-Ninth Annual IEEE*, 2014, pp. 2822-2827.
[43] R. I. Leine and H. Nijmeijer, *Dynamics and bifurcations of non-smooth mechanical systems* vol. 18: Springer Science & Business Media, 2013.
[44] M. Hallworth and S. A. Shirsavar, "Microcontroller-Based Peak Current Mode Control Using Digital Slope Compensation," *IEEE Transactions on Power Electronics,* vol. 27, pp. 3340-3351, 2012.
[45] S. Chattopadhyay and S. Das, "A Digital Current-Mode Control Technique for DC–DC Converters," *IEEE Transactions on Power Electronics*, vol. 21, pp. 1718-1726, 2006.
[46] A. O. Elbkosh, "Nonlinear Analysis and Control of DC-DC Converters," *PhD Thesis Newcastle University,* 2009.

Haimeng Wu (M'10) was born in Zhejiang, China, in 1986. He received the B.Sc. degree from Chongqing University, Chongqing, China, in 2008. He was nominated as the postgraduate exempted from the national postgraduate entrance examination to Zhejiang University and then he got the M.Sc. degree from College of Electrical Engineering, Zhejiang University, Hangzhou, China, in 2011. He received the grants from Engineering and Physical Science Council (EPSRC) for his further education in UK. In 2016, he got his Ph.D. degree at the School of Electrical and Electronic Engineering, Newcastle University, United Kingdom. He joined in Electrical Power Research Group at Newcastle University as a Postdoctoral Researcher since 2015. His current research interests include power electronics for electric vehicles and advanced nonlinear control.

Volker Pickert (M'04) studied Electrical and Electronic Engineering at the Rheinisch-Westfaelische Technische Hochschule (RWTH), Aachen, Germany and Cambridge University, UK. He received his Dipl.-Ing. degree from RWTH in 1994 and the Ph.D. degree from Newcastle University, Newcastle upon Tyne, U.K. in 1997.

From 1998 to 1999, he was Application Engineer with Semikron GmbH, Nuremberg, Germany and from 1999 to 2003 he was Group Leader at Volkswagen AG, Wolfsburg, Germany, responsible for the development of electric drives for electric vehicles. In 2003 he was appointed as a Senior Lecturer in the Electrical Power Research Group at Newcastle University and in 2011 he became Full Professor of Power Electronics. In 2012 he has become the Head of the Electrical Power Research Group. He has published more than 120 book chapters, journal and conference papers in the area of power electronics and electric drives. His current research interests includes power electronics for automotive applications, thermal management, health monitoring techniques and advanced nonlinear control.

Prof. Pickert is the recipient of the IMarEST Denny Medal for the best article in the Journal of Marine Engineering in 2011. He was chairman of the biannual international IET conference on Power Electronics, Machines and Drives in 2010 in Brighton and he is the active Editor-in-Chief of the IET Power Electronics journal.

Damian Giaouris – has received his PhD & MSc in the area of Control of Electrical Systems from Newcastle University (UK), Postgraduate Certificate & BSc in Mathematics from Open University (UK), and BEng in Automation Engineering from Technological Educational Institute of Thessaloniki (Greece). He was a Lecturer in Control Systems at Newcastle University since 2004, before moving to the Centre for Research and Technology Hellas (Greece) in 2011. Since September 2015 he is a Senior Lecturer in Control of Electrical Systems at Newcastle University. His research interests include control of power converters, power systems, smart grids, electric vehicles, and nonlinear dynamics of electrical systems. He has more than 115 publications (with more than 1400 citations), currently he is an associate editor of IET Power Electronics and he has been a Guest Associate Editor of IEEE Journal on Emerging and Selected Topics in Circuits and Systems.

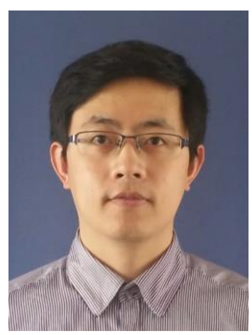

Bing Ji (M'13) received the M.Sc. and Ph.D. degrees in electrical and electronic engineering from Newcastle University, U.K., in 2007 and 2012 respectively. From 2012, he worked on the electrical powertrain and battery management systems of electric vehicles as a power electronics engineer with a UK low-emission vehicle company. He joined Newcastle University as a Postdoctoral Researcher in 2013, working on accurate power loss measurement and health management for power electronics. He is currently a Lecturer of Electrical Power Engineering with the University of Leicester. His research interests include reliability of power semiconductor devices, batteries and converters, function integration of gate drivers, electro-thermal modeling, thermal management and high power-density converter integration for electric vehicle applications. He is also a member of the IET.